doi:10.1006/jmbi.2001.5168 available online at http://www.idealibrary.com on IDEAL® *J. Mol. Biol.* (2002) **315**, 141–153

JMB

Crystal Structure Analysis of the Exocytosis-sensitive Phosphoprotein, pp63/parafusin (Phosphoglucomutase), from *Paramecium* Reveals Significant Conformational Variability

Simone Müller, Kay Diederichs, Jason Breed, Roland Kissmehl Karin Hauser, Helmut Plattner and Wolfram Welte*

Department of Biology University of Konstanz 78457 Konstanz, Germany

*Corresponding author

During exocytosis of dense-core secretory vesicles (trichocysts) in *Paramecium*, the protein pp63/parafusin (pp63/pf) is transiently dephosphorylated. We report here the structures of two crystal forms of one isoform of this protein which has a high degree of homology with rabbit phosphoglucomutase, whose structure has been reported. As expected, both proteins possess highly similar structures, showing the same four domains forming two lobes with an active-site crevice in between. The two X-ray structures that we report here were determined after crystallization in the presence of sulfate and tartrate, and show the lobes arranged as a closed and an open conformation, respectively. While both conformations possess a bound divalent cation, only the closed (sulfate-bound) conformation shows bound sulfate ions in the ''phosphate-transfer site'' near the catalytic serine residue and in the ''phosphate-binding site''. Comparison with the open form shows that the latter dianion is placed in the centre of three arginine residues, one contributed by subunit II and two by subunit IV, suggesting that it causes a contraction of the arginine triangle, which establishes the observed conformational closure of the lobes. It is therefore likely that the closed conformation forms only when a phosphoryl group is bound to the phosphate-binding site. The previously published structure of rabbit phosphoglucomutase is intermediate between these two conformers. Several of the known reversible phosphorylation sites of pp63/pf-1 are at positions critical for transition between the conformations and for binding of the ligands and thus give hints as to possible roles of pp63/pf-1 in the course of exocytosis.

Keywords: exocytosis; parafusin; *Paramecium*; phosphoprotein; phosphoglucomutase

Introduction

Among systems with dense-core vesicle exocytosis, the ciliated protozoan *Paramecium* operates faster and more synchronously[1] than any other cell.[2] In response to the polyamine secretagogue aminoethyldextran (AED), *Paramecium* releases almost all of its up to 1000 specialized secretory organelles (trichocysts) within 80 ms, as determined by quench-flow analysis.[1,3] This involves activation of a Ca^{2+}/(polyvalent cation)-sensing receptor, CaSR, Ca^{2+} mobilisation from subplasmalemmal stores (alveolar sacs) and store-operated Ca^{2+}-influx (SOC),[4,5] with the generation of a cortical $[Ca^{2+}]_i$ transient.[4,6] This is accompanied by

Present address: J. Breed, Astra Zeneca, Mereside, Macclesfield SK10 4TG, UK.

Abbreviations used: ASU, asymmetric unit; AED, aminoethyldextran; DLS, dynamic light scattering; ER, endoplasmic reticulum; Glc-1-P, glucose-1-phosphate; PEG-MME, polyethyleneglycol monomethyl ether; pf, parafusin; PGM, phosphoglucomutase; rmsd, root-mean-square displacement; SOC, store-operated Ca^{2+} influx; SR, sarcoplasmic reticulum.

E-mail address of the corresponding author: wolfram.welte@uni-konstanz.de

0022-2836/02/020141–13 $35.00/0

membrane fusion and content release, all within 80 ms, followed by endocytotic membrane resealing during ~350 ms.[3] Although CaSR and SOC-type mechanisms are known from widely different cell types,[7,8] important details concerning this signal transduction pathway have remained obscure.

During the 80 ms required for all exocytotic events in a cell suspension, there occurs the dephosphorylation of a 63 kDa phosphoprotein, pp63/parafusin (pf).[9] This is observed only in exocytosis-competent strains, although all strains analysed contain phosphorylated pp63/pf, even non-discharge mutants,[10] regardless of their widely different molecular defects.[11] Surprisingly, pp63/pf isolated from *Paramecium* displayed phosphoglucomutase (PGM, EC 5.4.2.2) activity.[12] PGM mediates transfer of a phosphate group between the C-1 and C-6 atoms of the glucose molecule before delivery into the glycolytic pathway.

In *P. tetraurelia*, there are at least two isoforms, pp63/pf-1 and pp63/pf-2. Both are likely to be expressed *in vivo*, and both have been sequenced and expressed as recombinant (non-phosphorylated) proteins in *Escherichia coli*.[13,14] The fact that pp63/pf-2 shows lower PGM activity than pp63/pf-1 (unpublished results) is surprising, since the two isoforms differ at only seven positions on the amino acid level, four of which represent conservative exchanges.[13] There is evidence of multiple phosphorylation of the two isoforms *in vivo*, by at least two different kinases.[14]

The crystal structure of the PGM from rabbit muscle, phosphorylated at the active-site serine residue, has been published.[15] The two crystallographically independent monomers are similar, and can be superimposed with a root-mean-square-displacement (rmsd) value of 0.71 Å (C^{α} atoms).

We report here the crystal structures of pp63/pf-1, unphosphorylated at the active-site serine residue, in complex with and without sulfate. As in the rabbit PGM crystals, both structures contain two crystallographically independent monomers that can be superimposed with low rmsd values. However, the structures with and without sulfate reveal a large conformational difference, and none of the two conformations resembles that of rabbit PGM.

On the basis of the crystal structures of the pp63/pf-1, we now try to set a baseline for several questions. (i) Can the new conformations observed in pp63/pf together with the existing PGM structure help to explain the catalytic cycle? (ii) How do the phosphorylation sites, as determined by matrix-assisted laser deionisation (MALDI) analysis,[14] map onto the structure of pp63/pf? (iii) Does the structure of pp63/pf-1 indicate a mechanism of activity regulation by phosphorylation? (iv) What kind of dimers are to be expected, considering occurrence of dimers in Western blots from cortical calcium stores (alveolar sacs)?[16] These aspects are important for defining a functional role in exocytosis for the observed rapid dephosphorylation of pp63/pf-1 in exocytosis-competent cells.

Results

Structure of pp63/pf-sulfate and comparison with the structure of rabbit PGM

Two different crystal forms of recombinant pp63/pf-1 (63,800 Da) were obtained, pp63/pf-sulfate in the presence of 0.2 M ammonium sulfate and pp63/pf-tartrate in the presence of 0.2 M sodium tartrate. Although both crystal forms belong to the same space group ($P2_12_12_1$) with two monomers per asymmetric unit (ASU), they exhibit grossly different unit cell constants (Table 1).

The structure of the sulfate crystal form was solved by molecular replacement using rabbit PGM as a search model.[15] As expected from the 50 % identity of residues of the search model with pp63/pf-1, the structure of the latter was very similar, showing the same overall V-shaped bilobal structure with approximate dimensions of 70 Å by 60 Å by 35 Å (Figure 1(a)) and the same four domains, I-IV, formed by residues 1-203, 204-322, 323-442 and 443-572 of pp63/pf-1, respectively. Equivalent domains of both proteins share common secondary structure elements and the same topology. Domains I-II together form a large lobe and domains III-IV a smaller lobe. Domain IV interacts with the concave face of its β-sheet with domain III. Figure 1(b) shows a structural alignment of both proteins using the abbreviations for secondary structure elements and loops introduced by Liu *et al*.[15]

The active-site cleft

The cleft between the two lobes forms the catalytic binding site for phosphoryl group transfer, which contains the catalytical Ser126 followed by His127 and Asn128 in the loop P of domain I in an arrangement reminiscent of the catalytic triad of serine proteases.[17,18] A close-up of the structure with details of the electron density map is shown in Figure 2(a). The distance between Ser126 O^{γ} and His127 $N^{\delta 2}$ is 2.7 Å. Asp310, Asp312 and Asp308 from loop M of domain II interact with the divalent cation, which is also near the catalytically active serine residue. Trp375 from domain III may be instrumental for providing a stacking interaction with the glucosyl group, as found in many binding sites for carbohydrates[19] (Figure 2(b)).

This active site is highly conserved in sequence and structure in both proteins, including the bound divalent cation. Under physiological circumstances, it is very probably Mg^{2+}, as this ion establishes the highest PGM activity *in vitro* (unpublished results; and see Ray *et al*,[20]), but refinement of the structure showed that a more electron-dense divalent ion results in slightly better *R*-factors. For this reason, we have tentatively modeled the bound ions as Ca^{2+} and Zn^{2+} in the

Table 1. X-ray data collection and refinement statistics

	pp63/pf-sulfate	pp63/pf-tartrate
A. *Data collection*		
X-ray source	BW7B, DESY, Hamburg	X-ray rotating anode, Schneider, Offenburg
Wavelength (Å)	0.8345	1.5415
Resolution limit (Å)	2.4 (2.40-2.49)	2.4 (2.40-2.50)
Unit cell *a*, *b*, *c* (Å)	67.3, 133.6, 150.5	64.9, 90.6, 212.0
Measured reflections	180,300 (11,572)	182,091 (10,401)
Unique reflections	50,610 (4304)	46,866 (3280)
Redundancy	3.6 (2.7)	3.9 (3.2)
Completeness (%)	94.2 (77.6)	94.6 (58.4)
I/σ	27.3 (11.9)	9.74 (3.1)
R_{meas} [a]	4.1 (8.5)	13.8 (44.3)
$R_{mrgd\text{-}F}$ [a]	3.0 (6.8)	13.7 (33.9)
B. *Refinement*		
rms bond length (Å)	0.007	0.007
rms angle deviation (deg.)	1.3	1.3
Ramachandran plot		
Core (%)	85.6	85.7
Allowed (%)	13.4	13.5
Generously allowed region (%)	0.7	0.5
Disallowed region (%)	0.3	0.3
R (30 Å-2.4 Å) (%)	23.3	22.7
R_{free} (30 Å-2.4 Å) (%)	28.4	28.6
Average *B*-factor (Å^2)	32.2	25.9
rms deviation between *B*-factors of bonded main-chain atoms (Å^2)	2.9	2.9

The numbers in parentheses are statistics from the highest shell.
[a] Defined as described.[50]

pp63/pf-tartrate and the pp63/pf-sulfate structure, respectively. However, Ni^{2+} and Mn^{2+} would fit the data equally well.

Several differences between the structures of pp63/pf-sulfate and of rabbit PGM are also noteworthy. Domains III-IV, which form the small lobe, associate differently with the domain I-II lobe and are relocated relative to the latter. This can be deduced from the rmsd values of overlays of the two lobes from both protein molecules of the asymmetric unit with the overlay of the whole proteins (Table 2, the last three columns in the second line). Roughly, in pp63/pf-sulfate the angle between the two lobes is smaller, resulting in a narrower active-site cleft. Interestingly, Liu *et al.*,[15] when comparing the two PGM molecules in the asymmetric unit, have also seen a subtle rearrangement of domain IV relative to domains I-III. In particular, those authors report a significant difference in the conformation of loop A between the two monomers, rendering one monomer more open than the other. The sequence of this loop is conserved in both pp63/pf isoforms and in rabbit PGM (see Figure 1(b)). In our structure, this loop

Table 2. Structural overlays of pp63/pf-1 and rabbit PGM. rmsd values in Å

	I	II	III	IV	I-II	III-IV	I-IV
pp63/pf-sulfate with pp63/pf-1-tartrate	0.36	0.46	0.48	1.19	0.61	1.53	2.30
pp63/pf-sulfate with rabbit PGM	1.23 (171)	0.60 (104)	0.67 (105)	1.04 (116)	1.17(282)	1.08 (229)	1.22 (515)
pp63/pf-tartrate with rabbit PGM	1.37 (179)	0.69 (104)	0.74 (110)	1.05 (114)	1.16(283)	1.29 (224)	1.43 (443)
Rabbit PGM, molecule A on B	0.36	0.31	0.41	0.90	0.36	0.74	0.71
pp63/pf-sulfate molecule A on B	0.20	0.26	0.23	0.31	0.24	0.38	0.42
pp63/pf-tartrate molecule A on B	0.25	0.31	0.32	0.43	0.43	0.47	0.57

For the rabbit PGM structure, the coordinates with accession number 3PMG deposited in the PDB bank were used. The rmsd values were calculated with LSQMAN[51] by using the domain definitions I = 2-203 for pp63/pf-sulfate and 3-203 for pp63/pf-tartrate, II= 204-322, III = 323-442, IV = 443-572, I-II = 1-322, III-IV = 323-572, I-IV = 1-572 and superimposing chain A of the two pp63-pf-1 crystal forms against each other and with chain A of rabbit PGM, or chain A with chain B for the comparisons within each dimeric structure. In those entries of the Table where a number is given in parentheses, this number refers to the number of superimposed C^{α} atoms after using the 'improve' option of LSQMAN with a distance cutoff of 3.8 Å. In all other cases, all C^{α} atoms in the domain were used.

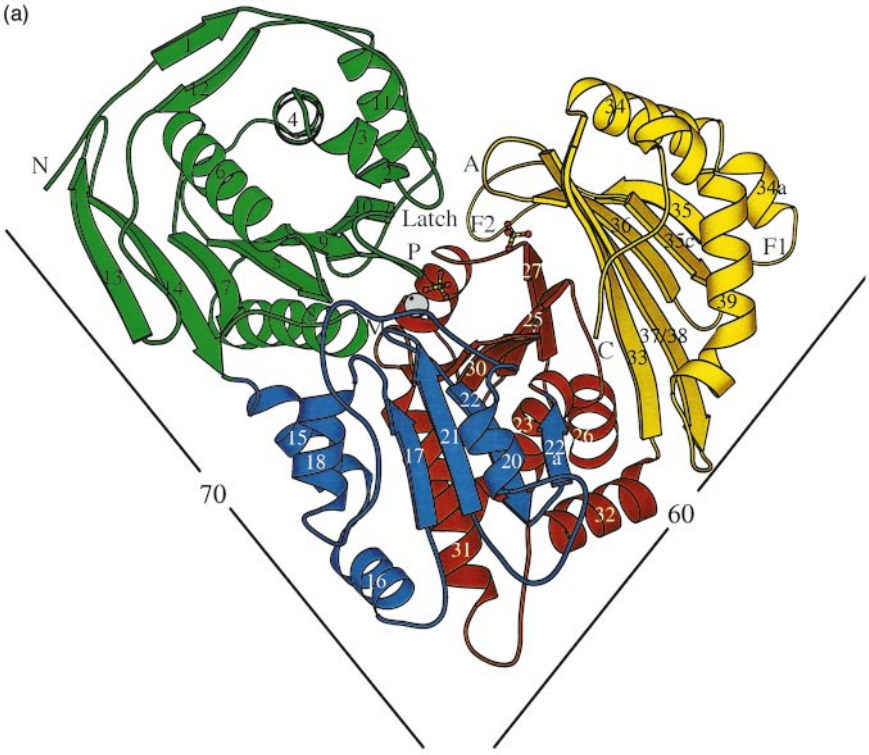

Figure 1 (*legend shown on page 162*)

has adopted a significantly different conformation, which allows for the narrowing of the active-site cleft compared to PGM without steric overlap with domain I. Thereby, loop A interacts directly with a segment on domain I (residues 23-27 between 1 and 2) for which we use the term latch (Figure 1(a)).

As a further difference, the phosphoserine residue found in the active site of PGM is replaced by a serine residue in pp63/pf-sulfate. An electron density peak 4.1 Å from the Ser126 O^{γ} is too far away to represent a phosphoryl group of phosphoserine. As the crystals were obtained in the presence of sulfate, it was modelled by us as sulfate-1. Three of the sulfate-1 oxygen atoms are about 4.5 Å apart from the serine oxygen atom and one is only 1.9 Å away from the divalent cation (Figure 2(b)). This sulfate-1 seems to occupy the proximal or phosphate transfer subsite.[15] Additional electron density is found in the active-site cleft between the catalytic serine residue with a particularly distinct peak near loop A. From its location near loop A, the molecular species there seems to occupy the distal or phosphate binding subsite.[15] As the density is found in the region where the substrates glucose 1-phosphate, glucose 6-phosphate and glucose 1,6-diphosphate are expected to bind, we assume that another sulfate ion has bound to the phosphate sites and thus we modeled the electron density peak as sulfate-2 (Figure 2(a)) in accordance with Liu *et al.*[15] Kuser *et al.*[21] also found a sulfate bound in hexokinase at the site where a phosphate was found in another conformation. Figure 2(b) shows the hydrogen bonding pattern of the two sulfate ions with partners. Arg27 and Ser24 are 8.7 Å and 3.9 Å apart from sulfate-1, respectively.

Another difference between pp63/pf-1 and rabbit PGM is in a 19 residue long peripheral surface-exposed segment after the first helix 34 of domain IV, which in PGM forms a loop containing the element termed F1 by Liu *et al.*[15] In pp63/pf-1, one part of this segment forms a kink in helix 34 and a subsequent short continuation of the helix (termed 34a by us) and another segment is absent, so that helix 34 is connected more closely with strand 35 (Figure 1(b)).

Comparison of the structures pp63/pf-sulfate and pp63/pf-tartrate

The structure of the pp63/pf-tartrate crystal form was solved by molecular replacement. While the structure of each of the four domains was rather similar to pp63/pf-sulfate, some rather significant differences became apparent when looking along the short axis of the molecule, i.e. the viewing direction of Figure 1(a). Domains I and II appear as a rigid scaffold, which is almost invariable. The domain IV lobe is attached with its con-

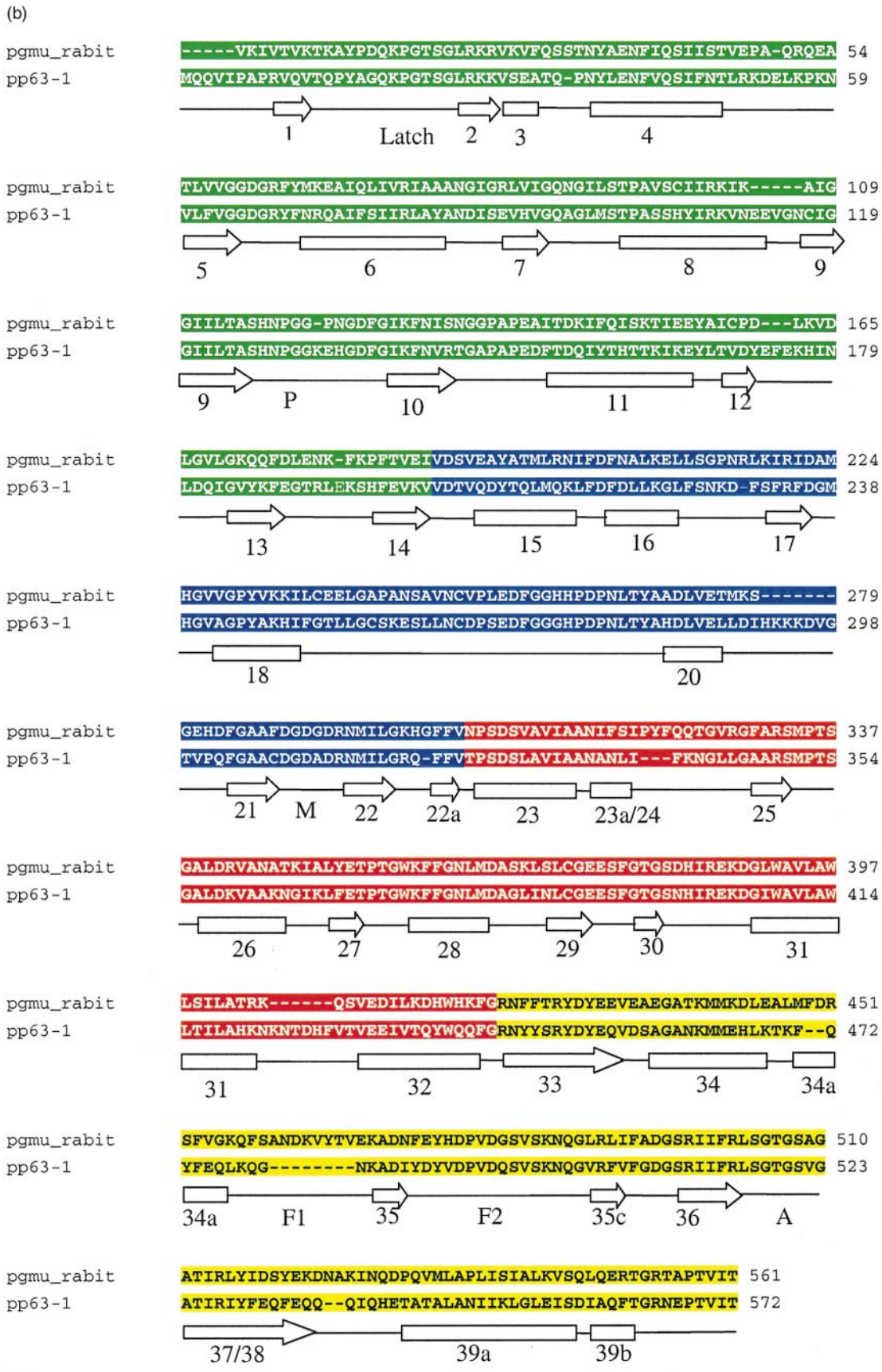

Figure 1 (*legend shown on page 146*)

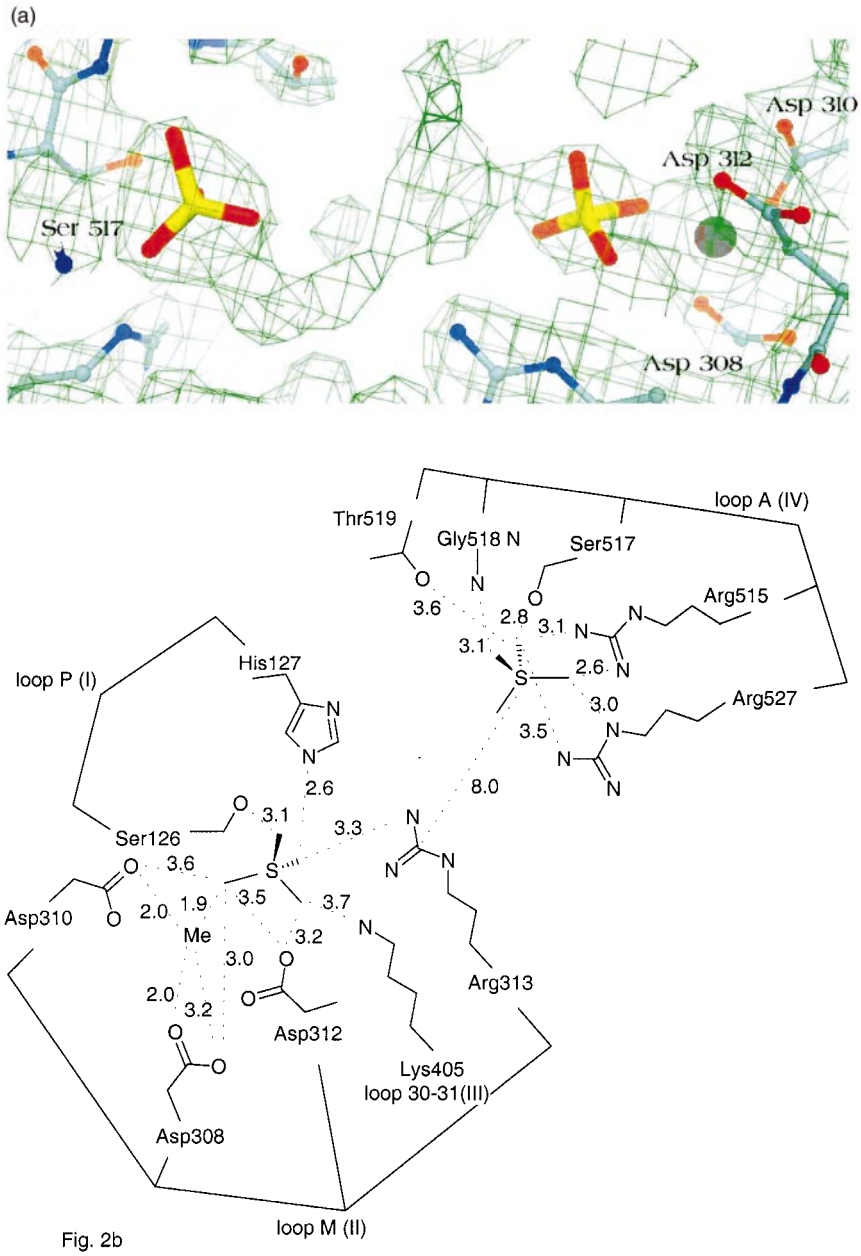

Figure 2. The active-site cleft and loop A. (a) Close-up of pp63/pf-sulfate with the electron density map. The active center with Ser126, the divalent cation (grey sphere) and sulfate-1 are shown on the right. Ser517 and sulfate-2 are shown near the lower left-hand corner. (b) Scheme of the arrangement of the sulfate ions, the divalent cation (Me) and protein residues with distances indicated in Å. Sulfate-1 is close to the following residues: Ser126 and His127, which are part of loop P in domain I; Asp308 , Asp310, Asp312 and Arg313, which are part of loop M between strands 21 and 22 of domain II; Lys 405, which is in a loop between strand 30 and helix 31 in domain III. Sulfate-2 is close to Arg515 and Arg527, which enclose loop A of domain IV. In this loop, the residues Ser517, Gly518, Thr519 are close to sulfate-2.

Figure 1. Structure of pp63/pf-sulfate and structural alignment with rabbit PGM. Important secondary structure elements and loops are labelled according to Liu *et al*.[15] In all subsequent Figures and Tables the domains are coded in the same colours as in (a). (a) Structure of the monomer in ribbon representation. The molecule is oriented to show the bilobal shape with the large lobe to the left and the small lobe to the right, and the approximate dimensions indicated in Å. Domains I, II, III, IV are coloured green, blue, red and yellow, respectively. The divalent cation and the two sulfate molecules are indicated as ball and stick models. (b) Structural alignment of pp63/pf-sulfate with PGM. This and all further structural Figures were prepared with MOLSCRIPT.[49]

cave β-sheet facing to domain III. It is both relocated and tilted with its tip away from domain I by approximately 5 Å, thus opening the cleft and increasing the angle between the two lobes (Figure 3). The conformational differences resemble those between pp63/pf-sulfate and PGM, but the displacements of domain IV relative to domains I-II are about twice as large.

The close association of loop A with the latch segment seen in pp63/pf-sulfate is entirely dissociated in pp63/pf-tartrate (Figure 3), so that residues from both loops have increased water-accessibility. Loop A undergoes the largest conformational transition in this movement. We have compared the water accessible surface of residues in pp63/pf-tartrate with pp63/pf-sulfate. Table 3 shows that in the latter, Thr23 and Arg27 of the latch segment and Asp493, Thr519 and Ser521 of loop A are partly sequestered from contact with water, as can be seen in Figure 3. The loop thus undergoes a strong conformational change relative to the rest of domain IV, continuing the above-mentioned trend seen between the structures of pp63/pf-sulfate and rabbit PGM. Domain III is also affected by the conformational change. This domain seems to be connected to domain IV. One noteworthy connection is a hydrogen bond between Thr373 OG1 from domain III (phosphorylated when pp63/pf-1 is isolated from cells) and Arg515 NH2 in domain IV, which is found in both crystal structures.

Table 3. Difference of the water-accessible surface of residues from the latch loop and from loop A between pp63/pf-tartrate and pp63/pf-sulfate (Å^2)

Latch loop		Loop A	
Thr23	33.5	Thr519	84.5
Arg27	38.0	Ser521	33.5

pp63/pf-tartrate shows density for the divalent cation near the catalytic serine residue, but does not show additional density in the active-site cleft as found in pp63/pf-sulfate, thus indicating that tartrate does not bind to the two sulfate-binding sites. Therefore, it is tempting to ascribe the energetics of the conformational transition to the electrostatic energy contribution of the sulfate ions. Indeed, sulfate-2 occupies a strategic position

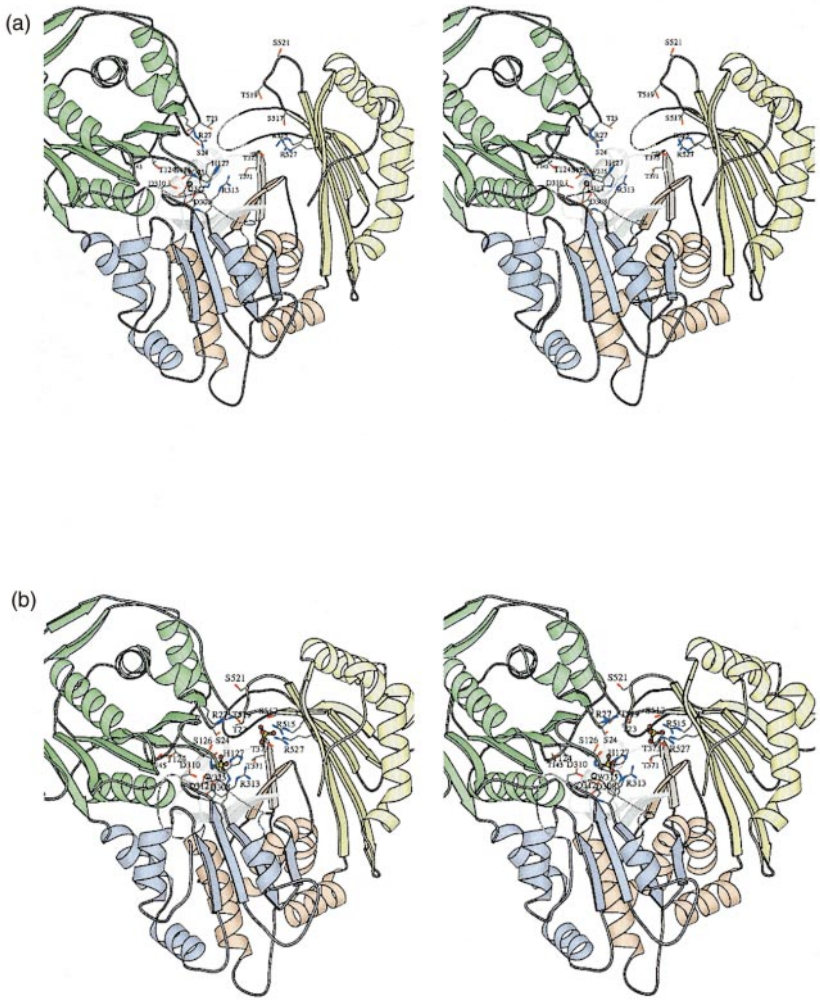

Figure 3. (a) The pp63/pf-tartrate and (b) the pp63/pf-sulfate structures in ribbon representation. The stereo views show the C^{α} carbon trace. Critical residues of the active site, the latch segment, loop A segment and others discussed in the text are shown and labelled.

within a triangle formed by three arginine residues, Arg313 from domain II and Arg515 as well as Arg527, both from domain IV (Figure 2(b)). The latter two enclose the loop A segment (residues 518-524, see Figure 1(b)). The distances between these arginine residues decrease by 2.1 Å, 2.8 Å and 2.3 Å, respectively, when comparing pp63/pf-tartrate with pp63/pf-sulfate. The sulfate-2 ion thus may act as a clip relocating domain IV and its loop A towards domain I.

Surprisingly, Liu *et al.*,[15] when substituting ammonium sulfate for PEG, did not observe a destruction of the crystals or any change in the crystal structure, although a sulfate ion obviously had occupied the distal phosphate-binding subsite. The intermediate PGM conformation, which persisted in the absence of divalent ions during crystallization, thus may have been stabilised by crystal-lattice forces. We thus presume that, while the binding energy of this ion favours the closed pp63/pf-sulfate conformation in solution, it does not suffice to do so in the PGM crystal lattice.

In summary, these results show that phosphoglucomutases can adopt larger and smaller interlobal angles than those reported for the rabbit PGM structure, revealing an open conformation in pp63/pf-tartrate, a closed conformation in pp63/pf-sulfate and an intermediate conformation in rabbit PGM.

The dimer

Western blots[16] and dynamic light-scattering studies (unpublished results) indicate the existence of pp63/pf-1 dimers. We therefore looked for plausible dimers in the crystal structure.

The ASU of both crystal forms contains an identical dimer structure with the domain I from two monomers apposed to each other, related to each other by a non-crystallographic 2-fold axis. This dimer possesses the largest surface buried from solvent among the dimers of the two crystal forms (2231 Å^2). According to Janin,[22] a buried surface larger than 900 Å^2 may indicate that the dimer is stabile in solution.

The interface is formed by apposition of the surface loops between strands 13 and 14 (domain I), helix 4 and strand 5 (domain I), strand 10 and helix 11 (domain I), helix 8 and strand 9 (domain I), helix 28 and strand 29 (domain III) and loop F2 (domain IV) of one molecule and and the symmetry-related corresponding loops of the apposed molecule. In the view shown in Figure 1(a) all these loops are on the rear surface. The interface contains salt-bridges and immobilised solvent molecules but no apparent clustering of hydrophobic residues.

Discussion

The two crystal structures of the *Paramecium* pp63/ppf-1 together provide strong evidence against a non-enzymatic regulatory role in trichocyst exocytosis. Exclusively, such roles have been ascribed to this protein during exocytosis regulation.[23–25] We can now endorse a role for the protein on the basis of its phosphorylation-modulated PGM activity. When the recombinant forms were tested, pp63/pf-1 had PGM activity comparable to that of rabbit muscle,[13] while pp63/pf-2 PGM had a somewhat lower activity (unpublished results).

Outlines of a possible reaction mechanism

The existence of three rather different conformations found in crystals structures of pp63 and rabbit PGM, i.e. pp63/pf-tartrate and pp63/pf-sulfate in this work and rabbit-PGM in Liu's work, represents a new challenge to deduce the events of the PGM-catalysed reaction from structure. As phosphate-binding sites can be occupied by sulfate ions,[26] and as the guanidinium groups of arginine residues are preferred interaction sites for them,[27] the structure of pp63/pf-sulfate appears to possess functional relevance. A valid mechanism must incorporate the fact that the transfer of the phosphoryl group between the C-1 O and the C-6 O atoms of glucose operates only after the active-site serine residue has been phosphorylated in the presence of glucose 1,6-diphosphate.[28] This indicates that the phosphorylation of the active-site serine residue by monophosphorylated glucose is unfavourable. We therefore presume that the phosphoryltransfer at the transfer subsite requires the presence of a phosphate group at the distal phosphate-binding site and we presume that the protein then is in a conformation similar to that of the pp63/pf-sulfate crystal structure.

The phosphoryl transfer from C-1 to C-6 could take place in two consecutive reactions. In a first reaction, the phosphoryl group of the active-site serine residue could be transferred to the 6 position of Glc 1-P which would be bound by its phosphate group to the distal binding site. The enzyme then would assume a more open conformation, possibly similar to the PGM crystal structure, which does not allow for dissociation of the substrate glucose diphosphate but allows for rearrangement so as to position the 1-phosphate group in the transfer site and the 6-phosphate group in the distal binding site. When this has been achieved, the protein may again assume a more closed conformation, similar to that of the pp63/pf-sulfate structure, to establish the cleavage of the phosphorylester bond with the C-1 O atom. Finally, the protein might assume a conformation similar to that of the pp63/pf-tartrate crystal structure, which allows for dissociation of the product.

Regulation of activity by phosphorylation

Although a precise function of the de-/re-phosphorylation cycle remains to be established, we know from MALDI-type mass spectrometry of *Paramecium* pp63/pf that this molecule is multiply

phosphorylated *in vivo*[14] and that transient dephosphorylation of pp63/pf is observed during trichocyst exocytosis.[9,10] Presently it has not been proved that the physiological phosphorylation state controls PGM enzymatic activity, but this appears highly probable on the basis of our present results.

In principle, three mechanisms can be envisaged: (i) steric inhibition of the ligand-binding site by phosphorylation; (ii) phosphorylation at sites critical for the conformational transitions taking place during the catalytic cycle; and (iii) allosteric inhibition or activation of the two above-mentioned processes by phosphorylation sites far from the active site. All of these mechanisms have been reported in enzymes.[27,29]

In detail, Thr23 on the latch (Figure 3), which is partly sequestered from solvent upon sulfate binding, is among the phosphorylated residues. Thr373 of domain III, hydrogen bonded to Arg515 in domain IV (N-terminal to loop A) in both conformations, is phosphorylated in native pp63/pf. We presume that the disruption of the hydrogen bond might reduce if not abolish the enzymatic activity. Thr24 of domain I close to Ser126 is phosphorylated in native pp63/pf. The introduction of two negative charges close to the active site likely interferes with the binding of substrates to the active site and with associated conformational changes (Figure 3). Loop A may be affected allosterically due to two flanking arginine residues, Arg515 and Arg527. The location of Thr371 suggests a similar role (Figure 3). Thr145 of domain I is partly buried upon sulfate binding with Asp383 from domain III. The phosphorylation of the former residue thus could interfere sterically with the conformational transition and affect the activity.

Cell biological background

As mentioned above, pp63/pf-1 dephosphorylation is strictly coupled to exocytosis (rapidly followed by endocytosis), so that pp63/pf seems to be involved in the regulation of these processes. Moreover, pp63/pf-1 is enriched in the *Paramecium* cortex according to immuno-gold labelling and Western blots from cell fractions, which also revealed some degree of structure binding.[16] The labelled sites include preformed exocytosis sites and the surface of surrounding subplasmalemmal Ca^{2+} stores (alveolar sacs). These display several features reminiscent of sarcoplasmic reticulum (SR) of skeletal muscle cells,[4,5] including Ca^{2+}-release channels sensitive to caffeine and 4-chloro-*m*-cresol, i.e. of the ryanodine-receptor type. According to quenched-flow and X-ray microanalysis, these stores are activated within 80 ms in response to AED,[30] thus inducing a store-operated Ca^{2+}-influx.[5] The time required for both, exocytosis and pp63/pf dephosphorylation is 80 ms.[9]

In conclusion, what could be the physiologic function of pp63/pf? One speculative aspect would be Ca^{2+} binding due to the multiple phosphorylation sites of pp63/pf-1. However, the phosphoglucomutase activity and the conformational changes we found give a strong hint that this catalytic performance and its regulation plays a functional role in the exocytosis events in *Paramecium*. The structural data further indicate that dephosphorylation by rendering the protein more similar to rabbit PGM should increase PGM activity. In this activated form, pp63/pf-1 could stimulate glycolysis, which in turn would stimulate respiration, thus providing energy for events accompanying exocytosis, e.g. to re-establish Ca^{2+} homeostasis. In fact, in *Paramecium*, stimulated exocytosis is accompanied by a significant ATP decay, followed by replenishment of the ATP pool,[31] the time-course being comparable to that of pp63/pf de- and rephosphorylation. A possibly similar situation may exist after muscle contraction when glycogenolysis and glycolysis may be of paramount importance[32–34] for Ca^{2+} transport. Indications exist that glycolytic enzymes are enriched in the small space between SR and plasmamembrane,[35] and in such narrow spaces ATP is regulated independent of bulk ATP.[36,37] Similarly, the space between alveolar sacs and the plasmamembrane in *Paramecium* is only ~15 nm wide.[38] Immediately below in the *Paramecium* cell cortex, mitochondria are enriched,[4] as is pp63/pf-1.[16]

In order to focus more carefully on the cytoplasmic ATP concentration or energy charge of the cell, we used our previously published (and some unpublished) data obtained with exocytosis-competent (exo $^+$) and exocytosis-incompetent (exo $^-$) strains. These phenotypes are related to the role of pp63/pf as dephosphorylation occurs only in exo $^+$ strains,[11] although the content of pp63/pf is very similar in all strains. In Table 4, we include all data on the extent of pp63/pf dephosphorylation[11] and ATP consumption and re-establishment of ATP homeostasis[31] during AED stimulation. It is seen that the strains contained in these two groups contain approximately the same amount of pp63/pf with a similar degree of phosphorylation, although only exo $^+$ group members dephosphorylate pp63/pf to any significant extent, i.e. 50 to 66 %. Upon AED stimulation, the time required to replenish 50 % (or 100 %) of the ATP pool depletion is much shorter in exo $^+$ than in exo $^-$ strains, i.e. 10.5 to 12.0 seconds (or ~30 s) in exo $^+$ *versus* 28.5 to 58 seconds (or >60 seconds) in exo $^-$ cells.

The exo $^+$ and the exo $^-$ group, respectively, each contains one strain with an unusually low basal concentration of ATP, namely strain K401 and nd9-28 °C, and both have to refill the highest ATP decay, i.e. 24.6 and 26.9 %, respectively. Nevertheless, the ATP recovery times are stereotypically the same for all exo $^+$ and exo $^-$ strains, respectively, and depend only on whether PP63/pf is dephosphorylated.

These observations are in accord with our suggestion that pp63/pf de-/rephosphorylation cycles may boost the synthesis of ATP, whose dramatic shortage may otherwise compromise cells. The actual phosphorylation state of pp63/pf would, of

Table 4. Comparison of exo $^{+}$ and exo $^{-}$ strains with regard to ATP dynamics and pp63/pf dephosphorylation

Strain	Relative ATP content[a]	%ATP consumption upon AED stimulation[b]	Time for 50 % ATP reformation (s)	Time for 100 % ATP reformation (s)	Relative degree of pp63/pf phosphorylation[a,c]	% Dephosphorylation of pp63/pf upon AED stimulation
A. *Exocytosis-competent strains*						
K401	0.45 ± 0.08	24.6 ± 1.8	12.0 ± 1.5	~30	0.86	−66
7S	**1.00** ± 0.26	13.8 ± 2.4	10.5 ± 1.5	~30	**1.00**	−54
d4-500r	1.05 ± 0.12	10.0 ± 2.6	11.5 ± 4.0	~30	1.00	−50
B. *Exocytosis-incompetent strains*						
nd9- 28 °C	0.58 ± 0.06	26.9 ± 2.4	28.5 ± 0.5	>60	1.21	+3
nd6	1.08 ± 0.23	8.5 ± 4.6	58.0[a]	⩾60	1.07	0
tl	1.09 ± 0.27	11.5 ± 4.2	28.5 ± 8.0	>60	0.97	0

±, Standard deviation, time in seconds. The 7S strain are wild-type cells; d4-500r lacks ciliary Ca^{2+}-channels and similarly strain K401 displays features irrelevant for exocytosis. For a more thorough characterization of strains, see Plathner & Klauke[4] and Vayssié *et al.*[10] ATP dynamics data are mostly from Vilmart-Seuwen *et al.*,[31] whereby strain nd9-18 °C has been omitted because of unusual culture temperature, while strain tam38 was omitted because (ATP) measurements had given no statistically significant results. The dephosphoylation data are from Zieseniss & Plattner.[11] All strains contain pp63/pf in phosphorylated form (normalized to to the value determined for 7S cells in unstimulated form, 1.00), the degree of its phosphorylation varies only slightly between the strains (between 0.86 and 1.21), and this variation is independent of exocytosis competence.

[a] Normalized to values for 7S, 1.00 = 1.2 mM ATP.

[b] Values of (ATP) observed at its lowest level, following three to six seconds of AED stimulation time.

[c] Maximal de-phosphorylation observed within one to five seconds of AED stimulation.

course, be the result of dynamic de- and rephosphorylation processes, and the observed net reaction is partial dephosphorylation. Due to the different phosphorylation sites, several different kinases must be involved, rendering it difficult to construct an *in vitro* model system.

Additional aspects, also concerning Ca^{2+} homeostasis, may be envisaged. PGM has been found in association with SR,[39,40] where it was suggested to regulate the opening state of Ca^{2+}-release channels depending on its phosphorylation state. In *Paramecium* cells, dimers of pp63/pf have been observed in Western blots from cortex fragments[16] and *in vitro* DLS data as well as the crystal structure provide further indications for dimer formation. In studies with yeast, Fu *et al*.[41] have studied the effects of PGM on Ca^{2+} homeostasis in the cytoplasm of *Saccharomyces cerevisiae* and on uptake into intracellular Ca^{2+} stores. They used wild-type cells and a mutant deficient in one of the two major PGM isoforms of these cells. The uptake of Ca^{2+} into the yeast cell, the ER and the Golgi indicated that glycolysis is co-regulated with Ca^{2+} transport and homeostasis. Glc 1-P may be a precursor of an unknown signal molecule that stimulates Ca^{2+}-uptake into the cell with or without prior depletion of the ER and Golgi Ca^{2+}-stores, as discussed by the above-mentioned authors. Another aspect worth considering is that, in a less active state, phosphorylation of several superficial residues of the PGM molecule could serve positioning in the cell,[42] in this case, in its cortex.[16]

Different roles of PGM could be in accord with our findings, although major functions and molecules of this regulatory system are unknown. This co-regulation of glycolysis and Ca^{2+}-transport would, in turn, be controlled on a higher level by phosphorylation of pp63/pf. To summarize, on the basis of data concerning localization, PGM activity and molecular structure, we assume an active role of pp63/pf, which is modulated during stimulated exocytosis by de- and rephosphorylation, in the context of Ca^{2+} signaling. Even though different mechanisms can be envisaged in detail, we underscore the energetic aspect and, thus, set a new baseline for future experiments. We assume that the strict correlation of the phosphorylation state with exocytosis performance is more than circumstantial.

Materials and Methods

Protein expression and purification

The overexpression and purification of recombinant, non-phosphorylated pp63/pf-1 has been reported.[13] For crystallization experiments, the protein was dialysed against 20 mM Tris-HCl (pH 7.5) buffer and concentrated to 10 mg/ml.

Crystallization and data collection

Two crystal forms of pp63/pf-1 were obtained by vapor diffusion in hanging drops. For each droplet, the protein solution (15 µl) was mixed with 5 µl of reservoir solution, containing 18 % (v/v) polyethylene glycol-monomethylether (PEG-MME) 2000 and 0.2 M ammonium sulfate in 0.1 M sodium acetate (pH 4.6) for the crystal form pp63/pf-sulfate, or 0.2-0.4 M sodium tartrate instead of ammonium sulfate for the crystal form pp63/pf-tartrate. The reservoir volume was 250 µl. After 10-14 days small crystals were visible and reached their final size of 700 µm × 300 µm × 300 µm after three to four weeks. Crystals were transferred to a cryoprotectant solution containing 20 % glycerol, 20 % PEG-MME, 0.1 M sodium acetate and either 0.1 M ammonium sulfate in the case of the pp63/pf-sulfate crystals or 0.1 M sodium tartrate in the case of pp63/pf-tartrate crystals), at pH 4.6 in either case, and frozen in liquid nitrogen.

Data from both crystal forms were collected on a home-based rotating anode and on the EMBL beamline BW7B at DESY (Hamburg), respectively. Both crystal forms are orthorhombic and belong to spacegroup $P2_12_12_1$, with two molecules per ASU (Table 1), but different cell axes.

Structure determinations, model building, and refinement

The structure of pp63/pf-1 was solved by molecular replacement. The structure of rabbit muscle PGM (PDB code: 3PMG) containing a covalently bound phosphate group and a Mg ion at the catalytic site, was used as a search model for the pp63/pf-sulfate data. The rotation function of the sulfate crystal form was calculated by the program BRUTELL,[43] and R. Read, unpublished. The highest rotation function solution was unambiguous; it stood out at 4.6 σ above the mean value. The translation function was obtained by CNS.[44] A model with the correct sequence was obtained by SWISS-MODEL[45] and it was transferred, using SUPERIMPOSE,[46] to the orientation and position found by molecular replacement. The refinement was started at an R_{free} value of 49.9 %. The structure of pp63/pf-tartrate was solved by molecular replacement, using the structure of the refined pp63/pf-sulfate crystal form.

Model building was performed using the program O[47] according to $|3F_{obs} - 2F_{calc}|$ and $|F_{obs} - F_{calc}|$ maps. Ramachandran plots were used for examination of the geometry.[48]

Cycles of structure refinement were carried out using CNS. Non-crystallographic symmetry restraints were set for each domain after optimizing domain borders by the program NCSGROUPS (K.D., unpublished). Water molecules were built into the model at sites with >2.5 σ peaks in electron density.

Protein Data Bank accession codes

Both models comprise residues 3-572 of native pp63/pf-1. The structure of the pp63/pf-sulfate crystal form contains in addition one divalent cation modelled as a Zn^{2+}, two sulfate ions and 205 water molecules. The structure of the pp63/pf-tartrate crystal form contains a divalent cation modeled as Ca^{2+} and 57 water molecules. The coordinates have been deposited in the RCSB Protein Data Bank (PDB accession codes 1KFI and 1KFQ).

Acknowledgements

We gratefully acknowledge financial support by a grant from the Deutsche Forschungsgemeinschaft to H.P.

References

1. Plattner, H., Knoll, G. & Pape, R. (1993). Synchronization of different steps of the secretory cycle in *Paramecium tetraurelia*: trichocyst exocytosis, exocytosis-coupled endocytosis, and intracellular transport. In *Membrane Traffic in Protozoa* (Plattner, H., ed.), pp. 123-148, JAI Press, Greenwich, London, UK, CT.
2. Kasai, H. (1999). Comparatiave biology of Ca^{2+}-dependent exocytosis: implications of kinetic diversity for secretory function. *Trends Neurosci.* **22**, 88-93.
3. Knoll, G., Braun, C. & Plattner, H. (1991). Quenched flow analysis of exocytosis in *Paramecium* cells: time course, changes in membrane structure, and calcium requirements revealed after rapid mixing and rapid freezing of intact cells. *J. Cell Biol.* **113**, 1295-1304.
4. Plattner, H. & Klauke, N. (2001). Calcium in ciliated protozoa: sources, regulation, and calcium-regulated cell functions. *Int. Rev. Cytol.* **201**, 115-208.
5. Klauke, N., Blanchard, M.-P. & Plattner, H. (2000). Polyamine triggering of exocytosis in *Paramecium* involves an extracellular Ca^{2+}/(polyvalent cation)-sensing receptor, subplasmalemmal Ca-store mobilization and store-operated Ca^{2+}-influx via unspecific cation channels. *J. Membr. Biol.* **174**, 141-156.
6. Klauke, N. & Plattner, H. (1997). Imaging of Ca^{2+} transients induced in *Paramecium* cells by a polyamine secretagogue. *J. Cell Sci.* **110**, 975-983.
7. Chattopadhyay, N., Yamaguchi, T. & Brown, E. M. (1998). Ca^{2+} receptor from brain to gut: common stimulus, diverse actions. *Trends Endocrinol. Metab.* **9**, 354-359.
8. Berridge, M. J., Lipp, P. & Bootman, M. D. (2000). The calcium entry pas de deux. *Science,* **287**, 1604-1605.
9. Höhne-Zell, B., Knoll, G., Riedel-Gras, U., Hofer, W. & Plattner, H. (1992). A cortical phosphoprotein ('PP63') sensitive to exocytosis triggering in *Paramecium* cells. Immunolocalization and quenched-flow correlation of time course of dephosphorylation with membrane fusion. *Biochem. J.* **286**, 843-849.
10. Vayssié, L., Skouri, F., Sperling, L. & Cohen, L. (2000). Molecular genetics of regulated secretion in *Paramecium*. *Biochimie.* **82**, 269-288.
11. Zieseniss, E. & Plattner, H. (1985). Synchronous exocytosis in *Paramecium* cells involves very rapid (<1 s), reversible dephosphorylation of a 65-kD phosphoprotein in exocytosis-competent strains. *J. Cell Biol.* **101**, 2028-2035.
12. Treptau, T., Kissmehl, R., Wissmann, J. D. & Plattner, H. (1995). A 63 kDa phosphoprotein undergoing rapid dephosphorylation during exocytosis in *Paramecium* cells shares biochemical characteristics with phosphoglucomutase. *Biochem. J.* **309**, 557-567.
13. Hauser, K., Kissmehl, R., Linder, J., Schultz, J. E., Lottspeich, F. & Plattner, H. (1997). Identification of isoforms of the exocytosis-sensitive phosphoprotein PP63/parafusin in *Paramecium tetraurelia* and demonstration of phosphoglucomutase activity. *Biochem. J.* **323**, 289-296.
14. Kussmann, M., Hauser, K., Kissmehl, R., Breed, J., Plattner, H. & Roepstorff, P. (1999). Comparison of in vivo and in vitro phosphorylation of the exocytosis-sensitive protein PP63/parafusin by differential MALDI mass spectrometric peptide mapping. *Biochemistry,* **38**, 7780-7790.
15. Liu, Y., Ray, W. J. & Baranidharan, S. (1997). Structure of rabbit muscle phosphoglucomutase refined at 2.4 Å resolution. *Acta Crystallog. sect. D,* **53**, 392-405.
16. Kissmehl, R., Hauser, K., Gössringer, M., Momayezi, M., Klauke, N. & Plattner, H. (1998). Immunolocalization of the exocytosis-sensitive phosphoprotein, PP63/parafusin, in *Paramecium* cells using antibodies against recombinant protein. *Histochem. Cell Biol.* **110**, 1-8.
17. Blow, D. M. (1997). The tortuous story of Asp . . . His . . . Ser: structural analysis of α-chymotrypsin. *Trends Biochem. Sci.* **22**, 405-408.
18. Perona, J. J. & Craik, C. S. (1997). Evolutionary divergence of substrate specificity within the chymotrypsin-like serine protease fold. *J. Biol. Chem.* **272**, 29987-29990.
19. Vyas, N. K. (1991). Atomic features of protein-carbohydrate interactions. *Curr. Opin. Struct. Biol.* **1**, 732-740.
20. Ray, W. J., Jr, Post, C. B., Liu, Y. & Rhyu, G. I. (1993). Structural changes at the metal ion binding site during the phosphoglucomutase reaction. *Biochemistry,* **32**, 48-57.
21. Kuser, P. R., Krauchenco, S., Antunes, O. A. C. & Polikarpov, I. (2000). The high resolution structure of yeast hexokinase PII with the correct primary sequence provides new insights into its mechanism of action. *J. Biol. Chem.* **275**, 20814-20821.
22. Janin, J. (1997). Specific versus non-specific contacts in protein crystals. *Nature Struct. Biol.* **4**, 973-974.
23. Andersen, A. P., Wyroba, E., Zhao, H., Reichman, M. & Satir, B. H. (1994). The activity of parafusin is distinct from that of phosphoglucomutase in the unicellular eukaryote *Paramecium*. *Biochem. Biophys. Res. Commun.* **200**, 1353-1358.
24. Levin, S., Almo, S. C. & Satir, B. H. (1999). Functional diversity of the phosphoglucomutase superfamily: structural implications. *Protein Eng.* **12**, 737-746.
25. Wyroba, E. & Satir, B. H. (2000). A comparative hybridization analysis of yeast DNA with *Paramecium* parafusin and different phosphoglucomutase-specific probes. *Biochem. Cell Biol.* **78**, 683-690.
26. Copley, R. R. & Barton, G. J. (1994). A structural analysis of phosphate and sulfate binding sites in proteins. *J. Mol. Biol.* **242**, 321-329.
27. Johnson, L. N. & O'Reilly, M. (1996). Control by phosphorylation. *Curr. Opin. Struct. Biol.* **6**, 762-769.
28. Voet, D. & Voet, J. G. (1995), *Biochemistry*, 2nd edit., J. Wiley, New York.
29. Johnson, L. N. (1992). Glycogen phosphorylase: control by phosphorylation and allosteric effectors. *FASEB J.* **6**, 2274-2282.
30. Hardt, M. & Plattner, H. (2000). Sub-second quenched-flow/X-ray microanalysis shows rapid Ca^{2+} mobilization from cortical stores paralleled by Ca^{2+} influx during synchronous exocytosis in *Paramecium* cells. *Eur. J. Cell Biol.* **79**, 642-652.
31. Vilmart-Seuwen, J., Kersken, H., Stürzl, R. & Plattner, H. (1986). ATP keeps exocytosis sites in a primed state but is not required for membrane

fusion. An analysis with *Paramecium* cells *in vivo* and *in vitro*. *J. Cell Biol.* **103**, 1279-1288.
32. Cuenda, A., Nogues, M., Gutiérrez-Merino, C. & DeMeis, L. (1993). Glycogen phosphorolysis can form a metabolic shuttle to support Ca^{2+} uptake by sarcoplasmic reticulum membranes in skeletal muscle. *Biochem. Biophys. Res. Commun.* **196**, 1127-1132.
33. Xu, K. Y., Zweier, J. L. & Becker, L. C. (1995). Functional coupling between glycolysis and sarcoplasmic reticulum Ca^{2+} transport. *Circ. Res.* **77**, 88-97.
34. Shulman, R. G. & Rothman, D. L. (2001). The ''glycogen shunt'' in exercising muscle: a role for glycogen in muscle energetics and fatigue. *Proc. Natl Acad. Sci. USA,* **98**, 457-461.
35. Han, J. W., Thieleczek, M., Varsány, M. & Heilmeyer, L. M. G. (1992). Compartmentalized ATP synthesis in skeletal muscle triads. *Biochemistry,* **31**, 377-384.
36. Landolfi, B., Curci, S., Debellis, L., Pozzan, T. & Hofer, A. M. (1998). Functional interactions between mitochondria and the ER measured in situ in intact cells. *J. Cell Biol.* **142**, 1235-1243.
37. Gribble, F. M., Loussouarn, G., Tucker, S. J., Zhao, C., Nichols, C. G. & Ashcroft, F. M. (2000). A novel method for measurement of submembrane ATP concentration. *J. Biol. Chem.* **275**, 30046-30049.
38. Plattner, H., Lumpert, C. J., Knoll, G., Kissmehl, R., Höhne, B., Momayezi, M. & Glas-Albrecht, R. (1991). Stimulus-secretion coupling in *Paramecium* cells. *Eur. J. Cell Biol.* **55**, 3-16.
39. Lee, Y. S., Marks, A. R., Gureckas, N., Lacro, R., Nadal-Ginard, B. & Kim, D. H. (1992). Purification, characterization, and molecular cloning of a 60-kDa phosphoprotein in rabbit skeletal sarcoplasmic reticulum which is an isoform of phosphoglucomutase. *J. Biol. Chem.* **267**, 21080-21088.
40. Coronado, R., Morrissette, J., Sukhareva, M. & Vaughan, D. M. (1994). Structure and function of ryanodine receptors. *Am. J. Physiol.* **266**, C1485-C1504.
41. Fu, L., Miseta, A., Hunton, D., Marchase, R. B. & Bedwell, D. M. (2000). Loss of the major isoform of phosphoglucomutase results in altered calcium homeostasis in *Saccharomyces cerevisiae*. *J. Biol. Chem.* **275**, 5431-5440.
42. Barinaga, M. (1999). New clues to how proteins link up to run the cell. *Science,* **283**, 124-125.
43. Fujinaga, M. & Read, R. J. (1987). Experiences with a new translation-function program. *J. Appl. Crystallog.* **20**, 517-521.
44. Brünger, A. T., Adams, P. D., Clore, G. M., DeLano, W. L., Gros, P., Grosse-Kunstleve, R. W. *et al*. (1998). Crystallography & NMR system: A new software suite for macromolecular structure determination. *Acta Crystallog. sect. D,* **54**, 905-921.
45. Guex, N. & Peitsch, M. C. (1997). SWISS-MODEL and the Swiss-PdbViewer: an environment for comparative protein modelling. *Electrophoresis,* **18**, 2714-2723.
46. Diederichs, K. (1995). Structural superposition of proteins with unknown alignment and detection of topological similarity using a six-dimensional search algorithm. *Proteins: Struct. Funct. Genet.* **23**, 187-195.
47. Jones, T. A., Zou, J. Y., Cowan, S. W. & Kjeldgaard, M. (1991). Improved methods for building protein models in electron density maps and the location of errors in these models. *Acta Crystallog. sect. A,* **47**, 110-119.
48. Laskowski, R. A., MacArthur, M. W., Moss, D. S. & Thornton, J. M. (1993). PROCHECK: a program to check the stereochemical quality of protein structures. *J. Appl. Crystallog.* **26**, 283-291.
49. Kraulis, P. J. (1991). MOLSCRIPT: a program to produce both detailed and schematic plots of protein structures. *J. Appl. Crystallog.* **24**, 946-950.
50. Diederichs, K. & Karplus, P. A. (1997). Improved *R*-factors for diffraction data analysis in macromolecular crystallography. *Nature Struct. Biol.* **4**, 269-275.
51. Kleywegt, G. J. (1999). Experimental assessment of differences between related protein crystal structures. *Acta Crystallog. sect. D,* **55**, 1878-1884.

Edited by D. Rees

(Received 19 June 2001; received in revised form 30 September 2001; accepted 10 October 2001)